

Higgs-portal Scalar Dark Matter: Scattering Cross Section and Observable Limits

Huayong Han and Sibong Zheng

Department of Physics, Chongqing University, Chongqing 401331, P. R. China

The simplest Higgs-portal dark matter model is studied in the light of dark matter self-interacting effects on the formation of large scale structures. We show the direct detection limits on the resonant and large mass regions. Finally, we also compare these limits with those at the LHC and Xenon 1T experiments.

I. INTRODUCTION

Scalar DM. The observed dark matter (DM) from galaxy rotation curves requires extension beyond the Standard Model (SM), where there is no viable candidate. Among other things, the simplest DM model corresponds to adding DM particle into the SM, with the SM Higgs scalar as the interaction mediator between these two sectors. This scenario is known as Higgs-portal DM. The direct detection limits at the LUX have excluded a fermion-like but still allow a scalar-like DM within mass range between 1 GeV and 10 TeV.

Detection. In the simplest scalar DM [1–4] there are only three model parameters, which include the DM mass m_s , Yukawa coupling constant κ_s between DM and Higgs scalar, and the DM self-interaction coupling constant λ_s . The signals of direct or indirect detection in this model are thus very predictive.

- **Indirect detection** mainly includes limits on DM annihilation into e^+e^- at PAMELA [5–7], into γ rays at Fermi-LAT [8], neutrinos in the sun [9–11], and possible Higgs invisible decay in the mass region $m_s < m_h/2$, where m_h refers to the Higgs mass.
- **Direct detection** mainly includes limits on the DM-nucleon spin-independent scattering at Xenon 100 [12] and LUX [13, 14], and the direct production at the LHC [15].

By combining all above experimental limits, one observes that the DM mass in the simplest scalar DM is constrained to two regions¹,

$$\begin{aligned} \text{resonant mass region : } 62.5 \text{ GeV} \leq m_s \leq 66 \text{ GeV,} \\ \text{large mass region : } m_s \geq 185 \text{ GeV.} \end{aligned} \quad (1)$$

Galactic Scale	limit (cm ² /g)	velocity (km/s)	Refs.
Milky Way	$\sigma/m_s \leq 1.0$	$\sim 10^2$	[24]
Cluster	$\sigma/m_s \leq 1.25$	$\sim 10^3$	[25]

TABLE I. Upper bounds on σ/m_s at different galactic scales inferred from DM self-interacting effects on the formation of LSS.

¹ If the Hubble parameter H during inflation is above 10^{16} GeV, the resonant mass region is totally excluded [16]. In contrast, these two regions are both consistent with present experimental limits if H is small enough. In this letter, we take the later assumption.

Self – interacting DM. In this paper we explore direct detection on this simplest model via self-interacting DM effects on the formation of large scale structures (LSS) [17], which is less studied in comparison with the DM-nucleon spin-independent scattering. As firstly described by Spergel and Steinhardt [18], self-interacting DM may be used to explain the constant core problem [19–23] and missing satellites in DM halos at the dwarf scale. In the former one, kinetic energy is transmitted from the hot outer halo inward because of DM self-interaction, with suitable strength described by σ/m_s , where σ denotes the scattering cross section for $ss \rightarrow ss$. In the later case, self-interaction could lead to satellite evaporation due to the DM particles within the satellites being kicked out by high-velocity encounters with DM particles from the surrounding dark halo of the parent galaxy.

Table I shows present limits on σ/m_s based on astrophysical observations at different galactic scales. The studies of DM self-interacting effects on the formation of LSS will shed light on two aspects. At first, the DM self-interaction coupling constant λ_s is constrained more efficiently, in compared with constraints arising from the DM relic density, direct detection limits at the LUX or LHC, which have little relevance to λ_s . Also, it provides the limits for discovery of DM in terms of astrophysical observations.

In Sec. II, we calculate the tree-level value for DM scattering cross section σ_0 in terms of Madgraph5 [26] and Feynman rules generator [27]. We eliminate parameter κ_s via the constraint from DM relic density, in terms of which σ_0 only depends on parameters m_s and λ_s . In Sec. III, we consider the Sommerfeld effect [28] on σ_0 due to the DM self-interaction [29–31]. In comparison with a massless or light-mass mediator, the Higgs mass upper bounds the enhancement factor significantly. The enhancement on the DM scattering cross section is verified to be mild in the resonant mass region, and less than $\sim 10^4 - 10^5$ in the large mass region for m_s above ~ 2 TeV. In Sec. IV we compare the experimental limits with those at the LHC and Xenon experiments.

Finally, we conclude in Sec. V.

II. TREE-LEVEL SCATTERING CROSS SECTION

In the simplest scalar DM model the relevant Lagrangian is given by,

$$\mathcal{L} = \frac{1}{2} (\partial s)^2 + \frac{\mu_s^2}{2} s^2 + \frac{\lambda_s}{2} s^4 + \frac{\kappa_s}{2} s^2 |H|^2. \quad (2)$$

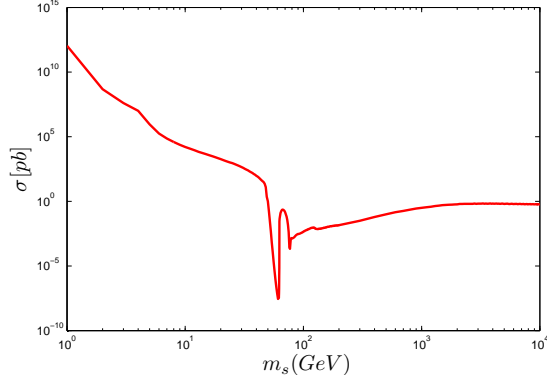


FIG. 1. The dependence of tree-level scattering cross section σ_0 due to Higgs mediator on DM mass ($\lambda_s = 0$). The dependence on κ_s is eliminated via the measured DM relic density [32].

Expand DM field s and Higgs field h along their vacuum expectation value $\langle s \rangle = 0$ and $\langle H \rangle = (v_{EW} + h)/\sqrt{2}$, respectively, we obtain

$$\mathcal{L} = \frac{1}{2}(\partial s)^2 + \frac{1}{2}m_s^2 s^2 + \frac{\lambda_s}{2}s^4 + \frac{\kappa_s v_{EW}}{2}s^2 h + \frac{\kappa_s}{4}s^2 h^2, \quad (3)$$

where $m_s^2 = \mu_s^2 + \kappa_s v_{EW}^2/2$. Here the electroweak scale $v_{EW} = 246$ GeV.

The contributions to the scattering cross section include two types of Feynman diagrams- one with intermediate Higgs scalar and the other with contact interaction. The tree-level value for σ_0 with and without quartic interaction is shown in Fig.1 and Fig.2, respectively, by using Madgraph5 [26]. In Fig.1 the dependence of σ_0 on κ_s is eliminated in terms of the measured DM relic density. Consequently, the total contribution to σ_0 , as shown in Fig.2, can be presented in the parameter space of m_s and λ_s . These numerical values are compatible with the analytic approximation in different mass limits [33],

$$\frac{\sigma}{10^4}[\text{pb}] \sim \begin{cases} 1.4 \cdot \lambda_s^2 \cdot \left(\frac{100 \text{ GeV}}{m_s}\right)^2, & m_s \gg m_h, \\ 5.6 \cdot \left(\frac{\lambda_s}{2} - \frac{\kappa_s^2 v^2}{8m_h^2}\right)^2 \cdot \left(\frac{100 \text{ GeV}}{m_s}\right)^2, & m_s \ll m_h. \end{cases} \quad (4)$$

Fig.2 indicates that σ_0 is upper bounded as $\sigma \leq 10^{12}$ pb in the whole range $0 \leq \lambda_s \leq 2$, which implies ² that $\sigma/m_s \leq 1 \text{ cm}^2/\text{g}$ for m_s above 1 GeV. Although small σ is compatible with the limits shown in Table I, relative larger σ is more favored in the light of direct detection at further astrophysical observations. As we will show in the next section,

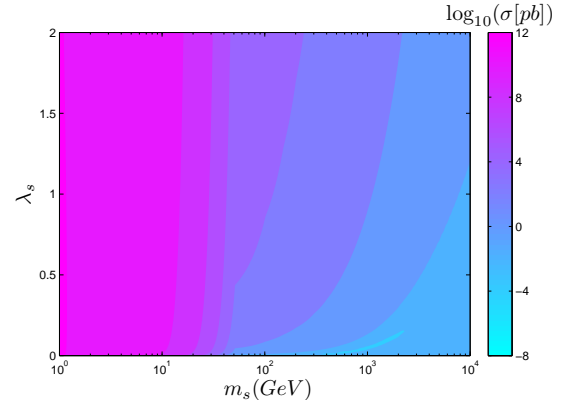


FIG. 2. Similar to Fig.1 but with quartic interaction included. Comparison with Fig.1 indicates that large λ_s dominates the contribution to σ_0 in the large mass region.

the Sommerfeld effect enhances the magnitude of σ_0 , which is as large as of order $\sim 10^4 - 10^5$ in the large mass region. It seems that the discovery potential for large mass region can be improved. This issue will be discussed in detail in Sec. IV.

III. SOMMERFELD EFFECTS

The S -wave annihilation cross section for two DM particles moving at small relative velocities, is enhanced by a factor (S) depending on the inverse velocity $v \sim 10^{-3}$, in compared with $v \sim 0.3$ at the freeze-out time. This enhancement is known as the Sommerfeld effect, which corresponds to the summation of a series of ladder diagrams with the mediator repeatedly exchanged. Since firstly applied to the wino dark matter [34], it has been clear that the DM annihilation cross section may be significantly differs from the DM scattering cross section when these two cross sections are both S -wave dominated.

This mediator is the Higgs scalar in our model. By following the works in [29–31], one obtains the enhancement factor in terms of solving the non-relativistic schrodinger equation,

$$-\frac{1}{m_s} \frac{d^2 \chi}{dr^2} + V(r) \chi = m_s v^2 \chi \quad (5)$$

where in our case the Yukawa potential ³,

$$V(r) = -\frac{\kappa_s^2}{4\pi r} \exp(-m_h r) \quad (6)$$

The boundary conditions are given by $\chi'(r) = im_s v \chi(r)$ and $\chi(r) \rightarrow \exp(im_s v r)$ when $r \rightarrow \infty$. Under such notation, the

² There is a useful relation among different units: $1 \text{ cm}^2/\text{g} = 1.8 \times 10^{12} \text{ pb}/\text{GeV} = 4.62 \times 10^3 \text{ GeV}^{-3}$.

³ A similar model has been considered in [35]. The Yukawa potential therein differs from ours due to different conventions.

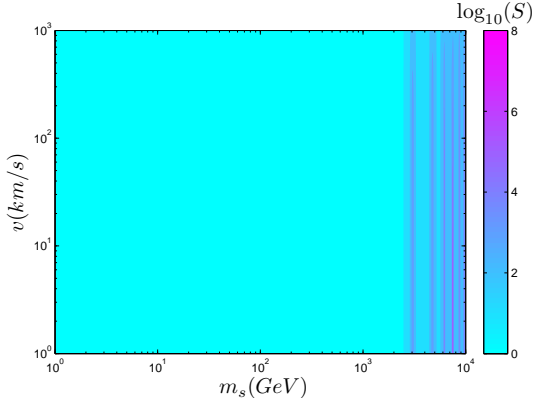


FIG. 3. Sommerfeld enhancement factor in the parameter space of m_s and v .

Sommerfeld enhancement factor S reads as,

$$S = \frac{|\chi(\infty)|^2}{|\chi(0)|^2} \quad (7)$$

which depends on parameters v and m_s .

Fig.3 shows our numerical solution to the Sommerfeld enhancement factor S in the parameter space of m_s and v . S is around unity for DM mass below 2 TeV, and its maximal value is about $\sim 10^5 - 10^7$ for $m_s \geq 3$ TeV. These numerical results agree with the analytic approximation [7, 30, 31],

$$S = \frac{\pi}{\epsilon_v} \frac{\sinh\left(\frac{2\epsilon_v}{\pi^2\epsilon_s/6}\right)}{\cosh\left(\frac{2\epsilon_v}{\pi^2\epsilon_s/6}\right) - \cos\left(2\pi\sqrt{\frac{1}{\pi^2\epsilon_s/6} - \frac{\epsilon_v^2}{(\pi^2\epsilon_s/6)^2}}\right)},$$

where $\epsilon_v = v/\alpha_{\kappa_s}$ and $\epsilon_s = m_h/\alpha_{\kappa_s}m_s$. Although it is not obvious in Fig.3, we have also verified the dependence that S decreases as the velocity v increases.

IV. COMPARISON WITH LHC AND XENON 1T

Combining the Sommerfeld effect gives rise to our final result on the DM scattering cross section σ ,

$$\sigma = S(v, m_s)\sigma_0(\lambda, m_s). \quad (8)$$

In terms of Fig.3 we plot σ/m_s as function of m_s for different λ_s and velocity v in the range of $10 - 10^3$ km/s in Fig.4. It is shown that the resonant mass region for large $\lambda_s \sim 2$ can be probed for σ/m_s of order $\sim 10^{-7}$ cm^2/g ; and σ/m_s of order $\sim 10^{-11}$ cm^2/g is required for small $\lambda_s \sim 0.1$. Smaller limits on σ/m_s are required for the detection for either smaller λ_s or larger DM mass.

Obviously, the value of σ/m_s is consistent with present astrophysical limits shown in Table I in the whole mass region. It is also obvious that the simplest Higgs-portal DM model can not provide σ large enough to explain the puzzles at the dwarf scale as mentioned in the introduction.

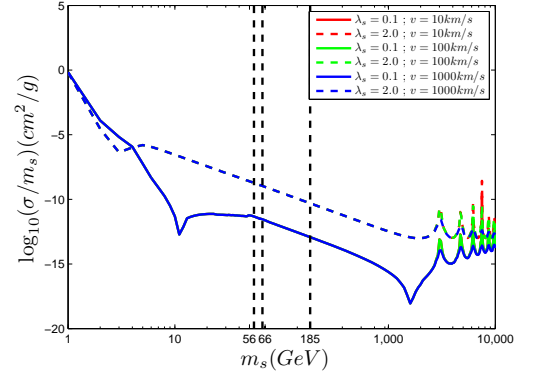


FIG. 4. σ/m_s as function of m_s for λ_s between 0.1 and 2 and $v = \{10, 10^2, 10^3\}$ km/s.

The required limits on σ/m_s for detection seems too small in compared with present limits (of order $\sim 10^{-1}$ cm^2/g). Does it imply that the astrophysical observations on LSS are less efficient in compared with other direct detection facilities? Let us compare these limits with those at the LHC and Xenon 1T experiments as required for discovery. The main observations are summarized in Table II. See what follows for explanation.

DM Mass (GeV)	LHC	Xenon 1T	LSS
Resonant mass region	✓	×	✓
Large mass region ($185 \leq m_s < 3000$)	×	✓	×
Large mass region ($m_s \geq 3000$)	×	×	×

TABLE II. Prospect for the discovery of DM at different experimental facilities. We have assumed that the limit on σ/m_s of order $\sim 10^{-7}$ cm^2/g can be reached in the further astrophysical observations on LSS. In comparison with the LHC, LSS provides a competitive way to detect the resonant mass region.

(i) As shown in Fig.5, the production cross section for DM at the 13-TeV LHC is less than $\sim 10^{-1}$ fb and 10^{-4} fb in the resonant mass region and the large mass region respectively. Therefore the later case is beyond the reach of LHC, and the former case can be detected only for extremely large integrated luminosity at least of order $\sim 10^3$ fb^{-1} if one takes care of the SM background.

(ii) The DM-nucleon spin-independent scattering cross section are less than $\sim 10^{-13}$ pb and $\sim 10^{-8}$ pb in the resonant mass region and large mass region with $m_s \geq 3$ TeV, respectively, which are both beyond the reach of Xenon 1T experiment [16].

(iii) With the assumption that the limit on σ/m_s of order $\sim 10^{-7}$ cm^2/g can be reached in the further astrophysical

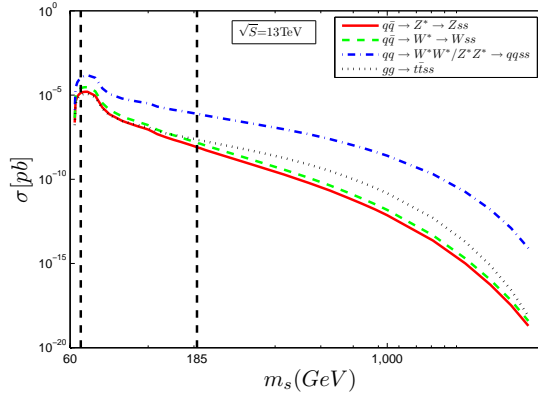


FIG. 5. Contributions to the production cross section for DM at the 13-TeV LHC, which are dominated by the vector boson fusion processes. The dependence on κ_s is eliminated similar to Fig. 1.

observations on LSS, the resonant mass region with large $\lambda \sim 2$ can be totally detected. Therefore, in comparison with the LHC, LSS provides a competitive way to detect the resonant mass region.

V. CONCLUSIONS

In this letter we have studied the DM scattering cross section in the simplest Higgs-portal DM model. We have also discussed the limits required for direct detection in terms of the astrophysical observations on LSS. We observe that (a) in compared with the LHC astrophysical observations on LSS provides a competitive way to detect the resonant mass region, which is beyond the reach of Xenon 1T experiment; (b) the large mass region with m_s above 3 TeV is beyond the reaches of all direct detections from the LSS, LHC and Xenon 1T.

Acknowledgement

This work is supported in part by Natural Science Foundation of China under Grant No.11247031 and 11405015.

[1] V. Silveira and A. Zee, Phys. Lett. B **161**, 136 (1985).
 [2] J. McDonald, Phys. Rev. D **50**, 3637 (1994), [hep-ph/0702143].
 [3] M. C. Bento, O. Bertolami, R. Rosenfeld and L. Teodoro, Phys. Rev. D **62**, 041302 (2000), [astro-ph/0003350].
 [4] C. P. Burgess, M. Pospelov and T. ter Veldhuis, Nucl. Phys. B **619**, 709 (2001), [hep-ph/0011335].
 [5] N. Arkani-Hamed, D. P. Finkbeiner, T. R. Slatyer and N. Weiner, Phys. Rev. D **79**, 015014 (2009), arXiv:0810.0713 [hep-ph].

[6] M. R. Buckley and P. J. Fox, Phys. Rev. D **81**, 083522 (2010), arXiv:0911.3898 [hep-ph].
 [7] J. L. Feng, M. Kaplinghat and H. B. Yu, Phys. Rev. D **82**, 083525 (2010), arXiv:1005.4678 [hep-ph].
 [8] M. Kaplinghat, T. Linden and H. B. Yu, Phys. Rev. Lett. **114**, no. 21, 211303 (2015), arXiv:1501.03507 [hep-ph].
 [9] C. S. Chen, G. L. Lin and Y. H. Lin, arXiv:1505.03781 [hep-ph].
 [10] J. Chen, Z. L. Liang, Y. L. Wu and Y. F. Zhou, arXiv:1505.04031 [hep-ph].
 [11] I. F. M. Albuquerque, C. Prez de Los Heros and D. S. Robertson, JCAP **1402**, 047 (2014), arXiv:1312.0797 [astro-ph.CO].
 [12] E. Aprile *et al.* [XENON100 Collaboration], “Dark Matter Results from 225 Live Days of XENON100 Data,” Phys. Rev. Lett. **109**, 181301 (2012), arXiv:1207.5988 [astro-ph.CO].
 [13] D. S. Akerib *et al.* [LUX Collaboration], “First results from the LUX dark matter experiment at the Sanford Underground Research Facility,” Phys. Rev. Lett. **112**, 091303 (2014), arXiv:1310.8214 [astro-ph.CO].
 [14] E. Del Nobile, M. Kaplinghat and H. B. Yu, arXiv:1507.04007 [hep-ph].
 [15] A. Djouadi, O. Lebedev, Y. Mambrini and J. Quevillon, Phys. Lett. B **709**, 65 (2014), arXiv:1112.3299 [hep-ph].
 [16] H. Han and S. Zheng, arXiv:1509.01765 [hep-ph].
 [17] M. Kaplinghat, S. Tulin and H. B. Yu, Phys. Rev. D **89**, no. 3, 035009 (2014), arXiv:1310.7945 [hep-ph].
 [18] D. N. Spergel and P. J. Steinhardt, Phys. Rev. Lett. **84**, 3760 (2000), [astro-ph/9909386].
 [19] A. Burkert, Astrophys. J. **534**, L143 (2000), [astro-ph/0002409].
 [20] V. Springel *et al.*, Mon. Not. Roy. Astron. Soc. **391**, 1685 (2008), arXiv:0809.0898 [astro-ph].
 [21] M. Vogelsberger, J. Zavala and A. Loeb, Mon. Not. Roy. Astron. Soc. **423**, 3740 (2012), arXiv:1201.5892 [astro-ph.CO].
 [22] M. Rocha *et al.*, Mon. Not. Roy. Astron. Soc. **430**, 81 (2013), arXiv:1208.3025 [astro-ph.CO].
 [23] O. D. Elbert, J. S. Bullock, S. Garrison-Kimmel, M. Rocha, J. Oorbe and A. H. G. Peter, Mon. Not. Roy. Astron. Soc. **453**, 29 (2015), arXiv:1412.1477 [astro-ph.GA].
 [24] M. Kaplinghat, R. E. Keeley, T. Linden and H. B. Yu, Phys. Rev. Lett. **113**, 021302 (2014), arXiv:1311.6524 [astro-ph.CO].
 [25] A. H. G. Peter, M. Rocha, J. S. Bullock and M. Kaplinghat, Mon. Not. Roy. Astron. Soc. **430**, 105 (2013), arXiv:1208.3026 [astro-ph.CO].
 [26] J. Alwall *et al.*, JHEP **1407**, 079 (2014), arXiv:1405.0301 [hep-ph].
 [27] A. Alloul *et al.*, Comput. Phys. Commun. **185**, 2250 (2014), arXiv:1310.1921 [hep-ph].
 [28] A. Sommerfeld, Annalen der Physik **403**, 257 (1931).
 [29] R. Iengo, JHEP **0905**, 024 (2009), arXiv:0902.0688 [hep-ph].
 [30] S. Cassel, J. Phys. G **37**, 105009 (2010), arXiv:0903.5307 [hep-ph].
 [31] T. R. Slatyer, JCAP **1002**, 028 (2010), arXiv:0910.5713 [hep-ph].
 [32] P. A. R. Ade *et al.* [Planck Collaboration], “Planck 2013 results. XVI. Cosmological parameters,” Astron. Astrophys. **571**, A16 (2014), arXiv:1303.5076 [astro-ph.CO].
 [33] R. Campbell, S. Godfrey, H. E. Logan, A. D. Peterson and A. Poulin, Phys. Rev. D **92**, no. 5, 055031 (2015), arXiv:1505.01793 [hep-ph].
 [34] J. Hisano, S. Matsumoto, M. Nagai, O. Saito and M. Senami, Phys. Lett. B **646**, 34 (2007) [hep-ph/0610249].
 [35] J. March-Russell, S. M. West, D. Cumberbatch and D. Hooper, JHEP **0807**, 058 (2008), arXiv:0801.3440 [hep-ph].